Identifying slip-slap forces in the contact interface using dual-mode excitation

F. Pourahmadian, H. Ahmadian, H. Jalali
Center of Excellence in Solid Mechanics & Dynamics
Iran University of Science and Technology
Narmak, Tehran, 16844, IRAN
Email: **ahmadian@iust.ac.ir**

Abstract
Frictional contact interfaces play a key role in dynamic behavior of mechanical systems. Various nonlinear mechanisms such as micro slap, micro and macro slippage develop at the frictional interface depending on the vibration amplitude at the contact surface. Majority of experimental studies consider the dynamic characteristics of the contact only in one direction, either tangential or normal. In the present paper, a procedure is proposed in which both components of the contact forces in these directions are simultaneously identified. The paper considers nonlinear behavior of a beam with frictional contact support as an experimental case study. The excitation force is set to dual sine harmonics and the measured responses are expanded using the beam nonlinear modes. This provides a reduced order model of the continuous system under study and forms the bases for identification of restoring forces in the contact interface. The restoring forces are identified using force state mapping technique and the hysteresis loops demonstrating the contact energy dissipation mechanisms are determined. The results demonstrate strong coupling effects between tangential and normal restoring forces and their dominant effects on the nonlinear characteristics of the contact interface in both directions.

1 Introduction

The effect of frictional contact interfaces on dynamic behavior of mechanical systems cannot be disregarded. Although a frictional contact at low vibration amplitudes is in stick regime and this leads to linear behavior of the system, many nonlinear mechanisms are associated with the contact behavior at higher amplitudes. In general investigations on contact interface dynamics can be categorized into three groups. Many studies consider the role of tangential component of the contact forces to characterize the frictional contact interface and assume a nearly constant normal load on the contact interface [1-5]. The second group focuses on frictionless contacts and inspects nonlinear attributes pertinent to normal force-displacement relationship at the contact [6-8]. Due to surface roughness at the interface, micro impact as well as micro and macro slippage develops as the level of vibration increases. Moreover, the tangential friction forces are strongly affected by the variation of normal contact force. In other words, the two components of the contact force have strong interactions. However, the number of experimental studies in this third group which concerns the nonlinear characteristics of the contact simultaneously in both directions, tangential and normal, is limited.

Literature on friction phenomenon is rich. Studies of Den Hartog [1] and Dowell [2] paved the way for the others in this field. In addition, thorough investigations on friction have been conducted by Ferri [3] and Berger [4]. Furthermore, a large number of models have been introduced to simulate the friction effects on mechanical systems. They are useful to gain a deep insight into nonlinear mechanisms involved in friction. A comprehensive overview on a range of constitutive models for joint interface has been provided by Gaul and Nitsche [5].

Surface roughness has a considerable effect on the normal force-displacement relationship. Assuming a distribution for the height of asperities, some models have been developed based on Hertzian theory [6] in

the normal direction. However, they are only concerned with nonlinear normal stiffness and damping characteristics are neglected. The most commonly used model to construct normal contact force with a nonlinear damping term has been proposed by Hunt and Crossley [7]. Y.Zhang and I.Sharf [8] tried to validate the Hunt and Crossley series of models using experimentally test data. They conclude that there is a need to develop new compliant models in normal direction capturing phenomenological mechanisms involved in impact damping such as plastic deformation.

In the present paper, a procedure is proposed in which the normal and tangential components of a frictional contact interface are identified simultaneously using experimental measurements. The nonlinear behavior of a beam with frictional contact support is considered in an experimental test study. Preload on the contact interface is set such that at the applied excitation force levels vibro-impacts develop in the frictional contact interface. The structure is excited in the vicinity of its first two resonance frequencies simultaneously using a dual harmonic input signal and a dual mode identification procedure is performed. The measured responses are expanded using the first two nonlinear modes of the system. These modes are defined as a combination of the base linear system mode shapes [9]. This procedure allows discretization of the continuous system and reduces its order to 2DOF. Eventually, the unknown components of the contact force are identified using force state mapping [10-11].

The remainder of this paper is organized as follows; the mathematical model of the system is presented in section 2. The experimental set-up and the test procedure are explained in section 3. The test set-up responses, measured in the experimental procedure, are employed in section 4 to identify the nonlinear modes and the restoring g forces at the contact interface.

2 Mathematical modeling

The structure considered in this paper is a fixed-frictionally supported uniform beam and its schematic diagram is shown in figure 1. A normal preload is applied to the contact interface using suspended mass blocks. In this study, the weight of mass blocks is selected such that the variation of the normal force in the contact interface is considerable. Therefore, the restoring forces in the contact interface consist of two components in normal and tangential directions.

The system consists of two parts; the beam which is the continuous part of the structure and the suspended mass blocks hanging from the beam end by a string. The dynamic behavior of the beam is modeled using Euler-Bernoulli beam theory. The beam has a modulus of elasticity of E, cross sectional moment of inertia of I, mass density of ρ, cross sectional area of A, and length of L. In this model, the axial inertial effects of the beam are neglected as the beam dynamic behavior of is considered in a frequency range much lower than its first axial mode. Therefore, in this direction the beam is modeled as a spring of stiffness $k_b = EA/L$. The frictional boundary support is provided by a pin welded to the beam end and the pin can slip on a steel surface. The pin has a radius of r, mass of m_p, mass moment of inertia of J_p. The mass blocks and the connecting string are modeled as a spring-mass system suspended from the beam end. The blocks mass is m_s and their mass moment of inertia is J_s. The string has a length of l_s and axial stiffness of k_s. The structure is excited using a concentrated force $f(t)$ at a distance d_p measured from its fixed end.

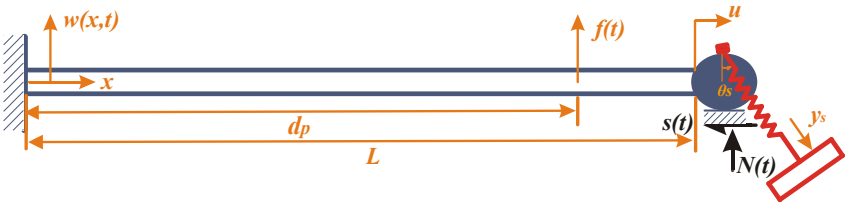

Figure 1- A slender beam with frictional support

The governing equations of the system under consideration are:

$$m_s\left(\ddot{u}-r\frac{\partial\ddot{w}(L,t)}{\partial x}+l_s\ddot{\theta}_s-\frac{\partial^2}{\partial t^2}\int_0^L\frac{1}{2}\left(\frac{\partial w}{\partial x}\right)^2dx\right)+k_bu+S(t)=0, \tag{1}$$

$$m_s\left(\ddot{w}(L,t)+r\frac{\partial\ddot{w}(L,t)}{\partial x}-\ddot{y}_s\right)-k_sy_s=0, \tag{2}$$

$$J_s\ddot{\theta}_s+m_sl_s\left(\ddot{u}-r\frac{\partial\ddot{w}(L,t)}{\partial x}+l_s\ddot{\theta}_s-\frac{\partial^2}{\partial t^2}\int_0^L\frac{1}{2}\left(\frac{\partial w}{\partial x}\right)^2dx\right)+m_sgl_s\theta_s=0, \tag{3}$$

$$EI\frac{\partial^4w}{\partial x^4}+\left(S(t)+m_s\left(\ddot{u}-r\frac{\partial\ddot{w}(L,t)}{\partial x}+l_s\ddot{\theta}_s-\frac{\partial^2}{\partial t^2}\int_0^L\frac{1}{2}\left(\frac{\partial w}{\partial x}\right)^2dx\right)\right)\frac{\partial^2w}{\partial x^2}+\rho A\frac{\partial^2w}{\partial t^2}=f(t)\delta(x-d_p). \tag{4}$$

Equation (1) describes the equilibrium state of the beam in axial direction, equations (2-3) govern the motions of the suspended mass blocks and the beam lateral vibration is governed by Euler-Bernoulli theory defined in equation (4). In equations (1-4), *w(x,t)* stands for the lateral displacement of the beam, *u* indicates the axial stretch in the beam, y_s represents the stretch in string holding the mass blocks and θ_s represents the blocks angular motions. These parameters are shown in figure 1. The tangential force *S(t)* takes into account the linear and non-linear characteristics of the contact shear force and *N(t)* stands for the contact normal force. The nonlinear characteristics involve both nonlinearities in stiffness and damping and are identified in this paper using experimental measurements.

The lateral motion partial differential equation (4) is subject to the following boundary conditions:

$$w(0,t)=0,\quad \frac{\partial w(0,t)}{\partial x}=0. \tag{5,6}$$

$$\begin{aligned}EI\frac{\partial^3w(L,t)}{\partial x^3}-m_p\left(\ddot{w}(L,t)+r\frac{\partial\ddot{w}(L,t)}{\partial x}\right)-m_s\left(\ddot{w}(L,t)+r\frac{\partial\ddot{w}(L,t)}{\partial x}-\ddot{y}_s\right)+N(t)\\+\frac{\partial w(L,t)}{\partial x}\left(S(t)+m_s\left(\ddot{u}-r\frac{\partial\ddot{w}(L,t)}{\partial x}+l_s\ddot{\theta}_s-\frac{\partial^2}{\partial t^2}\int_0^L\frac{1}{2}\left(\frac{\partial w}{\partial x}\right)^2dx\right)\right)=0.\end{aligned} \tag{7}$$

$$\begin{aligned}EI\frac{\partial^2w(L,t)}{\partial x^2}+rEI\frac{\partial^3w(L,t)}{\partial x^3}+rS(t)\left(1+\frac{\partial w(L,t)}{\partial x}\right)+J_p\frac{\partial\ddot{w}(L,t)}{\partial x}-\\rm_s\left(\ddot{u}-r\frac{\partial\ddot{w}(L,t)}{\partial x}+l_s\ddot{\theta}_s-\frac{\partial^2}{\partial t^2}\int_0^L\frac{1}{2}\left(\frac{\partial w}{\partial x}\right)^2dx\right)\left(1-\frac{\partial w(L,t)}{\partial x}\right)=0.\end{aligned} \tag{8}$$

The continuous model described in equations (1-4) is expanded using its associated nonlinear modes as:

$$\begin{Bmatrix}\overline{w}(x,t)\\ \overline{u}(t)\\ \overline{y}_s(t)\\ \overline{\theta}_s(t)\end{Bmatrix}=\sum_{i=1}^{n}\begin{Bmatrix}\tilde{\varphi}_i(x)\\ \tilde{u}_i\\ \tilde{y}_{si}\\ \tilde{\theta}_{si}\end{Bmatrix}q_i(t) \tag{9}$$

Descriptions of nonlinear modes $\tilde{\varphi}_i(x),\tilde{u}_i,\tilde{y}_{si},\tilde{\theta}_{si}$ employed in equation (9) are presented in section 4. This expansion series is substituted into nonlinear equations of motion (1-4) and the Galerkin method is applied to obtain the generalized coordinates $q_i(t)$. Projection of residues of equations (1-4) to the nonlinear modes of system results:

$$\begin{aligned}&\int_0^L\tilde{\varphi}_i(x)\left(EI\frac{\partial^4\overline{w}}{\partial x^4}+\left(S(t)+m_s\left(\ddot{\overline{u}}-r\frac{\partial\ddot{\overline{w}}(L,t)}{\partial x}+l_s\ddot{\overline{\theta}}-\frac{\partial^2}{\partial t^2}\int_0^L\frac{1}{2}\left(\frac{\partial\overline{w}}{\partial x}\right)^2dx\right)\right)\frac{\partial^2\overline{w}}{\partial x^2}+\rho A\frac{\partial^2\overline{w}}{\partial t^2}-f(t)\delta(x-d_p)\right)dx+\\&\tilde{u}_i\left(m_s\left(\ddot{\overline{u}}-r\frac{\partial\ddot{\overline{w}}(L,t)}{\partial x}+l_s\ddot{\overline{\theta}}_s-\frac{\partial^2}{\partial t^2}\int_0^L\frac{1}{2}\left(\frac{\partial\overline{w}}{\partial x}\right)^2dx\right)+k_b\overline{u}+S(t)\right)+\tilde{y}_{si}\left(m_s\left(\ddot{\overline{w}}(L,t)+r\frac{\partial\ddot{\overline{w}}(L,t)}{\partial x}-\ddot{\overline{y}}_s\right)-k_s\overline{y}_s\right)+\\&\tilde{\theta}_{si}\left(J_s\ddot{\overline{\theta}}_s+m_sl_s\left(\ddot{\overline{u}}-r\frac{\partial\ddot{\overline{w}}(L,t)}{\partial x}+l_s\ddot{\overline{\theta}}_s-\frac{\partial^2}{\partial t^2}\int_0^L\frac{1}{2}\left(\frac{\partial\overline{w}}{\partial x}\right)^2dx\right)+m_sgl_s\overline{\theta}_s\right)=0.\end{aligned} \tag{10}$$

The effects of boundary conditions (5-8) appear in the solution of the problem when integrations by part of equation (10) are performed twice. The generalized coordinates $q_i(t)$ and their time derivatives are obtained from measured responses using equation (9) and the exciting force *f(t)* is measured directly. Therefore, all the terms in equation (10), except for the contact restoring forces *S(t)* and *N(t)*, are known. Force state mapping technique is employed to identify these two unknown forces simultaneously using at least two modes that contribute in the system response considerably.

In order to plot hysteresis loops, the relative displacement in tangential and normal directions at the contact point is required. The relative tangential displacement is governed by three different effects as:

$$\xi(t) = -\frac{1}{2}\int_0^L \left(\frac{\partial w(x,t)}{\partial x}\right)^2 dx + r\frac{\partial w(L,t)}{\partial x} + u(t). \tag{11}$$

The first effect is related to shortening of the beam due to its lateral motion and is described by the first term on the right hand side of equation (11). The second term is the relative motion due to rotation of the beam end, and last term indicates the axial displacement of beam end due to friction force at the contact interface. The relative normal displacement at the contact point is defined as:

$$\eta(t) = w(L,t) + r\frac{\partial w(L,t)}{\partial x} \tag{12}$$

The first term in equation (12) is the beam lateral deflection at the contact interface and as the contact interface is located at distance *r* from the beam end, the rotation at this point provides the second term of equation (12).

In the next section, the experimental set-up and the test procedure are presented. The time signals recorded in the experiment are used to identify the nonlinear modes and the unknown components of the contact force.

3 Experimental case study

A steel beam of length *L=600 mm*, width *b=40 mm* and thickness *h=5 mm* clamped at one end and supported using a frictionally contact interface at the other end is employed in this experimental study. The pin welded to the beam end is steel and it has a radius of *r=6mm* and its length is equal to the beam width. A normal preload is applied to the contact interface using suspended mass blocks. The arranged set-up allows changing the preload if it is necessary. The structure is excited using a *B&K4200* mini shaker attached through a stinger to the beam at distance *S=550 mm* from the clamped end. A *B&K8200* force transducer is placed between stinger and the structure to measure the excitation force *f(t)*. Three accelerometers are mounted on the beam at locations x_1*=550 mm*, x_2*=300 mm* and *x3=50 mm* (measure from the beam clamped end). Figure 2 shows the test setup used in this experiment.

Figure 2: The test set-up of frictionally supported beam

The contact interface involves different nonlinear mechanisms depending on the vibration amplitude level. In low excitation amplitude levels the system behaves linearly. In this situation, the variation of normal contact force is negligible and in tangential direction the interface is in stick regime. Thus the contact interface can be modeled using two linear springs; one in normal and the other in tangential direction. As the excitation force level increases, nonlinear behavior develops not only in tangential direction due to micro and macro slippage but also in normal direction because of the micro slap.

In order to identify the unknown contact forces, the structure is excited near two of its base linear system natural frequencies simultaneously. The applied force *f(t)* has two harmonics; one near the first natural frequency and the second harmonic in the vicinity of the second resonance frequency. Exciting the structure near it resonance frequencies provides a considerable vibration in the structure without using high external force levels and the response of the structure is dominated by two harmonics. Furthermore, in this situation the mode shapes of the base linear system can be employed as good initial estimations of the nonlinear modes required in Galerkin discretization procedure.

Dynamic response of structure is measured while the preload on the contact interface is 7 *kg*. Figure 3 shows the driving point linear frequency response function recorded at low level of random excitation force. The corresponding natural frequencies are tabulated in table 1.

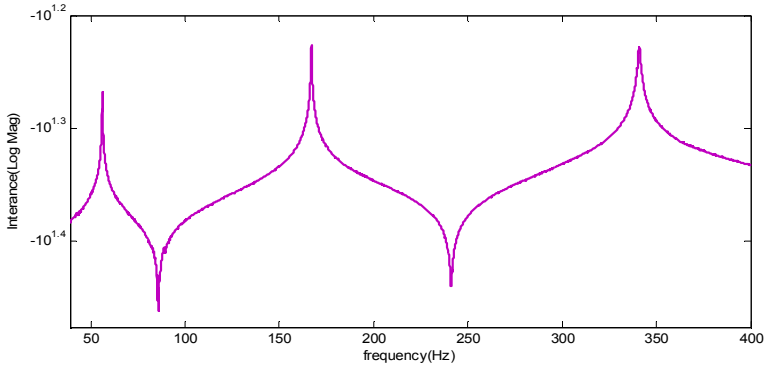

Figure 3: Driving point frequency response at low level excitations

ω_1	ω_2	ω_3
54.85	166.2	339.25

Table 1: Resonance frequencies at low level random excitations (Hz)

Next, the dynamic behavior of the structure is recorded while nonlinear mechanisms develop in the contact. The excitation is set to be dual sine in which four parameters, two amplitudes and two frequencies, change in each case to form the required force signal. The two corresponding phase were set to zero. In all cases, the first harmonic is set near the first natural frequency and the second one is tuned exactly three times as the first harmonic. This is due to the fact that the ratio between the first two modes of the base linear system is tuned into 1:3. In order to be sure that each mode has a definite contribution in the response, the force signal is tuned such that the amplitude of each harmonic in auto spectrum of the driving point acceleration signal remains constant. The procedure is repeated for some other excitation frequencies and level of vibrations near the resonant condition and in each case the system response is recorded. It is noteworthy that in this procedure neither the force time signal nor the time signal of acceleration is kept constant but the percentage of participation of each mode in the response is kept constant.

In the following section, the recorded signals are used to define the beam nonlinear modes and to identify the components of the contact interface restoring forces.

4 Evaluation of the test results

The measured force and acceleration signals are used in this section to reconstruct the nonlinear restoring forces in the contact interface. This reconstruction is performed using equation (10) requiring two nonlinear modes and the corresponding generalized coordinates $\ddot{q}_i(t), q_i(t)$, *i=1,2*. The first part of this section deals with determination of the nonlinear modes employed in the discretization procedure. In the second part measured accelerations and identified mode shapes are employed to calculate the generalized coordinates using equation (9).

The linear mode shapes of the system are employed to define the nonlinear modes. The modes of the base linear system are identified as follows. In the linear model the contact interface is modeled using two springs in normal and tangential directions, *i.e.* k_n, k_t. One obtains the governing equations of the base linear system by assigning the restoring forces *S(t)* and *N(t)* in equations (1-8) as:

$$S(t) = k_t\left(r\frac{\partial w(L,t)}{\partial x} + u(t)\right), N(t) = k_n\left(w(L,t) + r\frac{\partial w(L,t)}{\partial x}\right) \tag{13}$$

Now, the base linear system is completely described. Using the measured natural frequencies tabulated in table 1 and solving the characteristic equation of linear problem defined in this section, k_t and k_n are identified and are tabulated in table 2.

Parameter	k_t **(N/m)**	k_n **(N/m)**
Value	3.95e6	2.37e7

Table 2: Resonance frequencies at low level random excitations (Hz)

The mode shapes of linear system are obtained. Although these mode shapes are good candidates for Galerkin projection, by expanding the theory introduced by Szemplinska-Stupnicka [12] to a multi-harmonic situation not only a better estimation of nonlinear modes is obtained but also the identification procedure becomes more accurate. In order to estimate nonlinear modes, the response of the system is approximated by a two component expansion as:

$$\begin{Bmatrix} \bar{w}(x,t) \\ \bar{u}(t) \\ \bar{y}_s(t) \\ \bar{\theta}_s(t) \end{Bmatrix} = \begin{Bmatrix} \tilde{\varphi}_1(x) \\ \tilde{u}_1 \\ \tilde{y}_{s1} \\ \tilde{\theta}_{s1} \end{Bmatrix} a_1 \sin(\omega t + \psi_1) + \begin{Bmatrix} \tilde{\varphi}_3(x) \\ \tilde{u}_3 \\ \tilde{y}_{s3} \\ \tilde{\theta}_{s3} \end{Bmatrix} a_3 \sin(3\omega t + \psi_3). \tag{14}$$

Later in this section, this assumption on two component expansion approximation is verified. The coefficient vectors of the two harmonics in equation (14) are assumed to be real valued functions which are obtained using the mode shapes of the base linear system and experimental data.

In order to identify nonlinear modes described in equation (14), the response of the structure is expanded using the first *m* modes of the base linear system as follows:

$$\begin{Bmatrix} w(x,t) \\ u(t) \\ y_s(t) \\ \theta_s(t) \end{Bmatrix} = \sum_{i=1}^{m} \begin{Bmatrix} \varphi_i(x) \\ u_i \\ y_{si} \\ \theta_{si} \end{Bmatrix} p_i(t) \tag{15}$$

where $p_i(t)$ is the generalized coordinate and its coefficient vector is the corresponding linear mode shape of the system. One may employ the above relation and define a direct relation between measured accelerations and the corresponding generalized coordinates. Normally the number of mode shapes used in equation (15) may not exceed the number of independent measured vibration signals. The generalized coordinate coefficient vector can be calculated using the measured accelerations at j points, $j \geq m$, and the linear mode shape matrix as:

$$\ddot{p}(t)=\begin{Bmatrix}\ddot{p}_1(t)\\ \ddot{p}_2(t)\\ \vdots\\ \ddot{p}_m(t)\end{Bmatrix}=\begin{bmatrix}\varphi_1(x_1) & \varphi_2(x_1) & \cdots & \varphi_m(x_1)\\ \varphi_1(x_2) & \varphi_2(x_2) & \cdots & \varphi_m(x_2)\\ \vdots & \vdots & \ddots & \vdots\\ \varphi_1(x_j) & \varphi_2(x_j) & \cdots & \varphi_m(x_j)\end{bmatrix}^{+}\begin{Bmatrix}\ddot{w}(x_1,t)\\ \ddot{w}(x_2,t)\\ \vdots\\ \ddot{w}(x_j,t)\end{Bmatrix}=\boldsymbol{\Phi}^{+}\ddot{\mathbf{w}} \tag{16}$$

The superscript ()+ refers to pseudo inverse of the matrix. Note the accelerometers are located on the beam and the discrete generalized coordinates, u_i, y_{si} and θ_{si} are not included in the mode shape matrix of equation (16). Next a Fourier series of the following form is fitted to every generalized acceleration signal:

$$\ddot{p}_i(t)=\sum_{k=1}^{K}A_{ki}sin(k\omega t+\psi_{ki})=A_{1i}sin(\omega t+\psi_{1i})+A_{3i}sin(3\omega t+\psi_{3i}),\ \ i=1,2,...,m. \tag{17}$$

Coefficients A_{ki} and ψ_{ki} are obtained from data fitting (see [13] for more details). The generalized displacement $p_i(t)$ is obtained by performing time integrations of equation(17) twice as:

$$p_i(t)=-\sum_{k=1}^{K}\frac{A_{ki}}{(k\omega)^2}\sin(k\omega t+\psi_k)=-\frac{1}{\omega^2}\left(A_{1i}\sin(\omega t+\psi_{1i})+\frac{A_{3i}}{9}\sin(3\omega t+\psi_{3i})\right),\ \ i=1,2,...,m. \tag{18}$$

The assumption about the nonlinear modes to be real valued functions can be verified provided each harmonic in the series expansion of the generalized coordinates has the same phase. Indisputably, if this condition is not met, the nonlinear modes in equation (14) are complex rather than real. In the case under consideration, this condition is fulfilled and the maximum phase difference between the corresponding phases is less than 10°. Subsequently, ψ_1 is substituted for ψ_{1i} and ψ_3 is replaced ψ_{3i}. By substituting $p_i(t)$ obtained from equation (18) into equation (15) one arrives at:

$$\begin{Bmatrix}w(x,t)\\ u(t)\\ y_s(t)\\ \theta_s(t)\end{Bmatrix}=-\frac{1}{\omega^2}\left(\sum_{i=1}^{m}A_{1i}\begin{Bmatrix}\varphi_i(x)\\ u_i\\ y_{si}\\ \theta_{si}\end{Bmatrix}\sin(\omega t+\psi_1)+\frac{1}{9}\sum_{i=1}^{m}A_{3i}\begin{Bmatrix}\varphi_i(x)\\ u_i\\ y_{si}\\ \theta_{si}\end{Bmatrix}\sin(3\omega t+\psi_3)\right). \tag{19}$$

and the nonlinear modes of equation (14) are obtained as:

$$\begin{Bmatrix}\tilde{\varphi}_j(x)\\ \tilde{u}_j\\ \tilde{y}_{sj}\\ \tilde{\theta}_{sj}\end{Bmatrix}=\frac{1}{\sqrt{A_{j1}{}^2+A_{j2}{}^2+...+A_{jm}{}^2}}\sum_{i=1}^{m}A_{ji}\begin{Bmatrix}\varphi_i(x)\\ u_i\\ y_{si}\\ \theta_{si}\end{Bmatrix},\ j=1,3. \tag{20}$$

Next the focus is turned into the experimental results. The system is excited in the vicinity of its first two natural frequencies. Consequently, it is not expected that a large number of modes contribute to the system response. Based on this estimation, the number of linear mode shapes m in equation (20) is set to three. In other words, three linear mode shapes used to identify two nonlinear modes. The corresponding generalized coordinates, $p(t)$, of this three modes is shown in figure 4; the amplitude of the first harmonic of the acceleration signal is set to 20(m/s^2) and the amplitude of the second harmonic is 50(m/s^2). In this situation the system experiences the largest amplitude of vibration in these experiments and hence the most deviation of nonlinear modes from the linear mode shapes is expected.

As it can be seen in figure 4 the third linear mode has a marginal contribution in the final shape functions. One must make sure that there is no need for considering more linear modes in defining the nonlinear ones. In this regard, the response at the driving point is reconstructed using nonlinear modes obtained by equation (20 and is compared with the measured accelerations in figure 5. There is an excellent agreement between the measured and predicted responses.

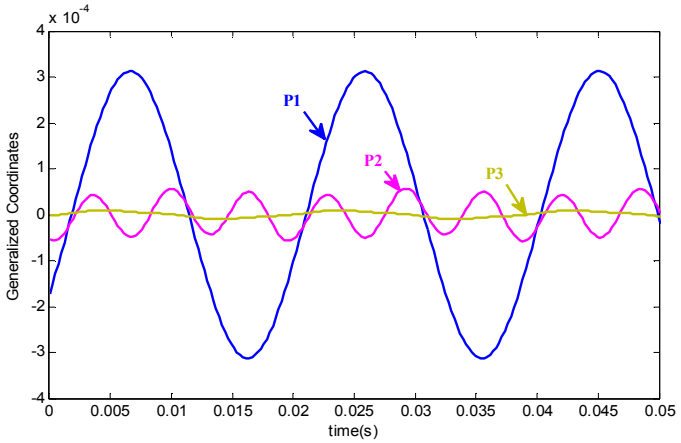

Figure 4: The generalized coordinates *vs.* time

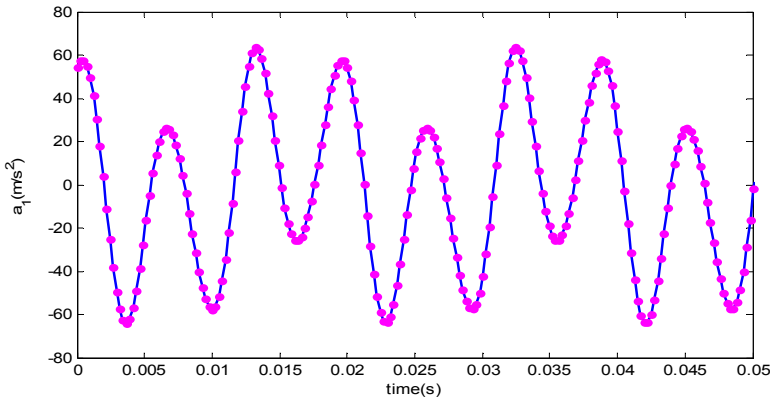

Figure 5: Accelerations at the driving point, measured (solid line) and reconstructed (circles)

At this point, all prerequisites for calculation of nonlinear restoring forces *S(t)* and *N(t)* using force state mapping are available. In this regard, two nonlinear modes obtained by equation (20) are employed to accomplish the Galerkin discretization procedure employed in equation (10). At each moment there are two equations for two unknown forces. Therefore, by solving these equations one can identify the contact forces using force state mapping. The deformations $\xi(t)$ in tangential direction and $\eta(t)$ in normal direction at the contact interface are defined in equations (11-12). Figure 6 shows the obtained force *vs.* displacement at each direction for three different amplitudes. In this figure a_1 is the amplitude of first harmonic of acceleration signal at the driving point while a_2 is the amplitude of second harmonic. It should be noted that the identified contact forces shown in figure 6 are expanded using Fourier series in time domain up to fifth harmonic as these harmonics appear in the generalized coordinates $q_1(t)$ and $q_2(t)$.

Since two main harmonics contribute in the system response, each hysteresis loop shown in figure 6 consists of three loops. In the normal direction, there is a hardening effect in the contact stiffness which is related to the surface roughness [6]. A number of models have been introduced so as to address this effect in the normal force-displacement relationship. However, to the knowledge of the authors, no phenomenological model has been proposed yet which simulates the nonlinear damping mechanism in the normal direction. On the tangential direction, the contact interface experiences micro and macro-slippage. Although the obtained hysteresis loops in tangential direction reveal general similarities to those proposed by some friction models such as Valanis model [14] and Iwan model [15], one should remember these models do not consider the normal force variations while in the case under consideration the normal force considerably changes.

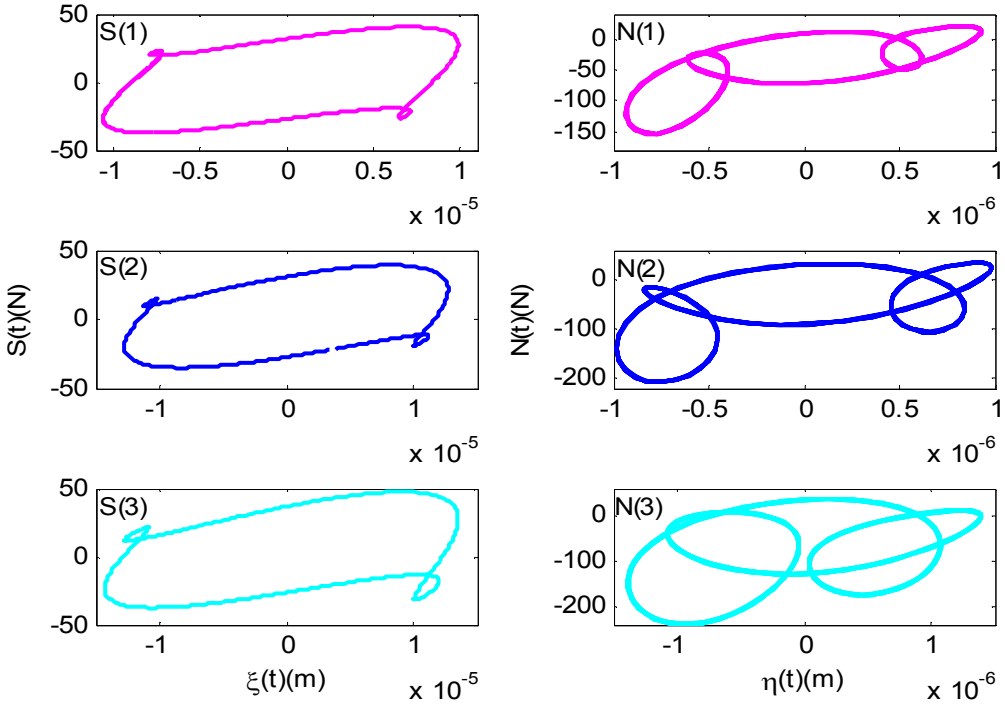

Figure 6: Identified contact restoring forces, S(1)- N(1) at a_1=14(m/s^2), a_2=34(m/s^2), S(2))- N(2) at a_1=17.5(m/s^2), a_2=42.5(m/s^2), S(3))- N(3) at a_1=20(m/s^2), a_2=50(m/s^2)

5 Conclusion

Dynamic characteristics of a beam with frictional contact support are investigated in situations in which the nonlinear mechanisms of micro slap, micro and macro slippage develop in the contact interface. The base linear system is set by the proper arrangement of the transducers in a way that the first two natural frequencies are near commensurable. The components of a dual sine excitation force are tuned such that the first two independent mode shapes of system have considerable contributions in the response. The system nonlinear modes are employed to expand the system responses and to identify the components of the contact force. The relative displacements in normal and tangential directions of the contact support are calculated and are used along with identified restoring forces to draw hysteresis loops. The results form a base to characterize the nonlinear effects and judge about their coupling effects. As no prior contact model is employed in identification procedure the hysteresis loops can be used as a tool to investigate the alteration of friction forces due to micro slaps and experimental validation of phenomenological 2D contact models.

References

[1] JP. Den Hartog, *Forced vibrations with combined Coulomb and viscous friction*, Trans ASME: Applied Mechanics, Vol. 53, Academic Press (1931), pp. 107-15.

[2] E. H. Dowell, *Damping in beams and plates due to slipping at the support boundaries*, Journal of Sound and Vibration, Vol. 105, Academic Press (1986), pp. 243-253.

[3] A.A. Ferri, *Friction damping and isolation systems*, Journal of Mechanical Design, Vol. 117, Academic Press (1995), pp. 196-206.

[4] E.J. Berger, *Friction modeling for dynamic system simulation*, Applied Mechanics Reviews, Vol. 55, Academic Press (2002), pp. 535-577.

[5] L. Gaul, R. Nitsche, *The role of friction in mechanical joints*, Applied Mechanics Reviews, Vol. 52, Academic Press (2001), pp. 93-106.

[6] W. Sextro, *Dynamical contact problems with friction, models, methods, experiments and applications*, Springer-Verlag, Berlin, Heidelberg (2007).

[7] K.H. Hunt, F.R.E. Crossley, *Coefficient of Restitution Interpreted as Damping in Vibro-impact*, Journal of Applied Mechanics, Vol. 42, Academic Press (1975), pp. 440-445.

[8] Y. Zhang, I. Sharf, *Validation of nonlinear viscoelastic contact force models for low speed impact*, Journal of Applied Mechanics, Vol. 76, Academic Press (2009), pp. 051002-1-12.

[9] F. Pourahmadian, H. Jalali, H. Ahmadian, *Identifying normal modes of a nonlinear system*, submitted to International conference on recent advances in structural dynamics, the Southampton, The England, 2010 July 12-14, The Southampton (2010)

[10] S.F. Masri, T.K. Caughey, *A nonparametric identification technique for nonlinear dynamic problems*, Journal of Applied Mechanics, Vol. 46, Academic Press (1979), pp. 433-447.

[11] A. Crawley, *Identification of nonlinear structural elements by force-state mapping*, AIAA, Vol. 24, Academic Press (1986), pp. 155-162.

[12] W. Szemplinska-Stupnicka, *The modified single mode method in the investigations of the resonant vibrations of nonlinear systems*, Journal of Sound and Vibration, Vol. 65, Academic Press (1979), pp. 475-489.

[13] K. Worden, G.R. Tomlinson, *Nonlinearity in Structural Dynamics: Detection, Identification and Modeling*, Institute of Physics Publishing, Bristol and Philadelphia (2001).

[14] K.C. Valanis, *A theory of visco-plasticity without a yield surface*, Archives of mechanics, Vol. 23, Academic Press (1971), pp. 171-191.

[15] W.D. Iwan, *A distributed-element model for hysteresis and its steady-state dynamic response*, ASME Journal of Applied Mechanics, Vol. 33, Academic Press (1966), pp. 893-900.